AD-A055 359 GEORGIA INST OF TECH ATLANTA SCHOOL OF CHEMICAL ENGI--ETC F/G 11/6
CYCLIC DUCTILITY, CYCLIC STRENGTH AND FATIGUE CRACK PROPAGATION--ETC(U)
MAY 78 S B CHAKRABORTTY N00014-75-C-0349

UNCLASSIFIED TR-78-2 NL

| OF |
AD
A055359

END
DATE
FILMED
7-78
DDC

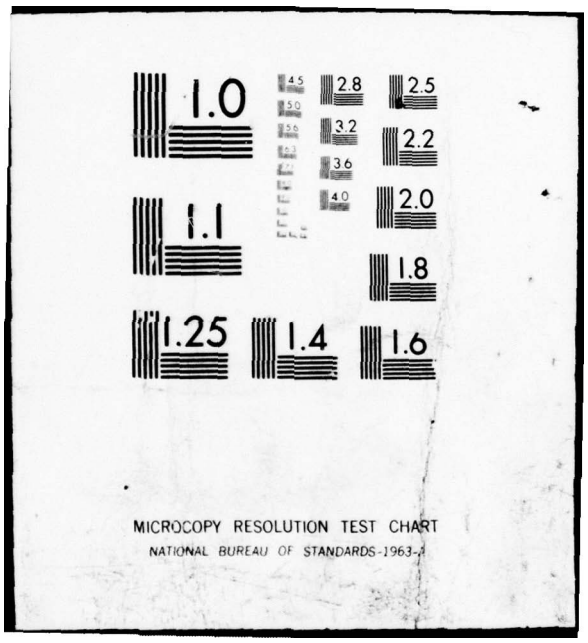
1.0
1.1
1.25
1.4
1.6
1.8
2.0
2.2
2.5
2.8
3.2
3.6
4.0
4.5
5.0
5.6
MICROCOPY RESOLUTION TEST CHART
NATIONAL BUREAU OF STANDARDS-1963-A

(12) SC

OFFICE OF NAVAL RESEARCH

Contract N00014-75-C-0349, NR 031-75
(15)

(9) TECHNICAL REPORT 78-2

(14) TR-78-2

(6) CYCLIC DUCTILITY, CYCLIC STRENGTH AND FATIGUE CRACK PROPAGATION OF METALS AND ALLOYS.

(10) BY
Saghana B. Chakrabortty

(11) 16 May [redacted]78

(12) 34p.

METALLURGY PROGRAM, SCHOOL OF CHEMICAL ENGINEERING
GEORGIA INSTITUTE OF TECHNOLOGY
ATLANTA, GEORGIA 30332

406 387

CYCLIC DUCTILITY, CYCLIC STRENGTH AND FATIGUE CRACK PROPAGATION OF METALS AND ALLOYS

ABSTRACT

Fatigue crack propagation has been related to the cyclic stress-strain and life-strain response of materials by means of a ductility exhaustion mechanism. The da/dn-ΔK relationship has been derived from the assumption that an elemental crack extention occurs when the sum of the fractional fatigue life of an element at various cycles is equal to unity. Experimental fatigue crack propagation data of representative metals and alloys have been compared with that predicted from their low cycle fatigue properties. The threshold ΔK behavior has been explained in terms of the existance of a threshold plastic strain amplitude.

INTRODUCTION

Fatigue crack propagation (FCP) has been studied on various materials for the last two decades. It has been almost universally recognized that fatigue crack propagation for a particular material is a function of the stress intensity factor, and experimental results are normally presented as log plots of fatigue crack growth rate (FCGR) per cycle (da/dn) versus the stress intensity factor range (ΔK) as shown schematically in Figure 1. An engineering material spends a negligible fraction of its life in region III and this stage is of least interest. There is a threshold ΔK_{th} value below which the crack does not measurably grow. The da/dn increases rapidly after ΔK_{th} and is sensitive to both the environment and the K_{max}:K_{min} ratio (R ratio). The ΔK_{th} decreases and da/dn value increases with the R ratio. A similar change also occurs when the environment is made more aggressive. There is an intermediate range of ΔK (Region II) where the crack growth data appears to follow the Paris[1] equation:

$$da/dn = A\ (\Delta K)^p \qquad (1)$$

Experimental results[2-6] have shown that the exponent p varies from two to four. Various attempts have been made to calculate the da/dn values from monotonic and cyclic properties of materials and also to calculate the exponent p of equation (1)[7-17]. However there has been little concentrated effort to find a theoretical basis for ΔK_{th}, to predict da/dn values for low ΔK region, or to explain the effect of R ratio and environment on the crack propagation rate.

Liu and Iino[13] assume that cumulative damage by strain cycling causes the crack to propagate. The material of a finite element in the reverse plastic zone (RPZ) ahead of the crack-tip experiences cyclic strain of increasing magnitude as the crack propagates toward it. If each cycle produces damage to

the material and if one uses Miner's[18] cumulative damage law and Coffin-Manson's[19,20] cyclic life-strain response (CLSR) law, an expression for FCGR may be derived. Liu and Iino[13] arrived at an equation for da/dn with p = 2. This is not satisfactory even for the intermediate ΔK range, since in reality p may vary from 2 to 4. Majumdar and Morrow[12] modified Liu and Iino's approach by introducing a microstructure parameter, ρ^*. They argue that continuum mechanics and bulk properties cannot be used to analyze a zone up to a distance of ρ^* ahead of the crack tip. Then they simply ignore the part of the fatigue life experienced by the material in this zone even though it experiences the most acute fatigue cycling. In some cases (especially at lower ΔK) this zone may become an appreciable fraction of the reverse plastic zone and Majumdar and Morrow's modification drastically reduces the da/dn calculated for the lower ΔK values. This results in an increase in the exponent p from the constant value of 2 predicted by Liu and Iino. However, one cannot ignore this important area ahead of the crack tip just because the analysis does not hold. In this paper a modification of the same Liu and Iino[13] model is used and the fatigue crack propagation behavior is correlated with CLSR and CSSR (cyclic stress-strain response) parameters (i.e., low cycle fatigue data) without ignoring any part of the RPZ ahead of the crack tip.

THE PROPOSED FATIGUE CRACK PROPAGATION MODEL

Fatigue Crack Propagation Rate: It is assumed that the reverse plastic zone ahead of a propagating crack tip is composed of small elements which undergo uniaxial cyclic plastic deformation. Crack extension occurs due to the exhaustion of cyclic ductility in these elements. The dimension of each element along the crack path is taken as the crack extension per cycle (da/dn). The

cyclic strain amplitude of an element ($\Delta\varepsilon$) depends upon its distance (x) from the crack tip and the applied stress intensity range (ΔK).

In order to estimate the relationship between $\Delta\varepsilon$ and x, Majumdar and Morrow[12] used Rice's[9] model for a stationary crack loaded in antiplane shear (mode III) under small scale yielding. From an analogy between mode I and III they derived

$$\Delta\sigma \cdot \Delta\bar{\varepsilon} = \frac{\Delta K^2}{(1+n')\pi E x} \tag{2}$$

where $\Delta\sigma$ and $\Delta\bar{\varepsilon}$ are the cyclic stress and strain ranges at a distance x from the crack tip,

n' is the cyclic strain hardening exponent, and

E is Young's modulus.

The strain amplitude can be divided into plastic and elastic components

$$\begin{aligned}\Delta\bar{\varepsilon} &= \Delta\bar{\varepsilon}_e + \Delta\bar{\varepsilon}_p \\ &= \frac{\Delta\sigma}{E} + \Delta\bar{\varepsilon}_p\end{aligned} \tag{3}$$

Assuming that $\Delta\bar{\varepsilon}_e$ is negligible compared to $\Delta\bar{\varepsilon}_p$ and that there is no effect of the strain amplitude calculated by equation (2) for $x \leq \rho^*$ (where ρ^* is the "microstructure size") Majundar and Morrow[12] deduced an equation for FCGR which may be written as

$$\frac{da}{dn} = 2 \int_{\rho^*}^{R_p} \left(\frac{\Delta\bar{\varepsilon}}{2\varepsilon'_f}\right)^{-\frac{1}{c}} dx \tag{4}$$

where R_p is the RPZ size, and c and ε'_f are the cyclic ductility exponent and cyclic ductility co-efficient (the CLSR parameters) respectively. The lower limit

of integration in (4) was assumed to be ρ^* because it was considered the lower limit for x, below which continuum analysis and bulk fatigue properties are not applicable. However, this author feels that the contribution of the cyclic strain within the distance of ρ^* ahead of the crack tip may not be negligible and the model presented herein used the following approach to incorporate the effect of this strain.

Assuming that cyclic stress and strain may be related by the CSSR parameters k' and n' from

$$\Delta\sigma = k'(\Delta\bar{\varepsilon}_p)^{n'} \tag{5}$$

and using equations (2), (3) and (5) we obtain:

$$x = \frac{A}{(\Delta\bar{\varepsilon}_p)^{n'} + \frac{k'}{E}(\Delta\bar{\varepsilon}_p)^{2n'}} \tag{6}$$

where $A = (\Delta K^2) / (1+n')\pi Ek'$. Equation (6) should predict the approximate cyclic plastic strain for a continuum, and represents strain as a continuously decreasing function of distance. However, in metals and alloys, this is an over-simplification, and may result in a significant error. For example, let us consider the deformation around a crack tip in a single phase polycrystalline material deforming by planar slip. Slip bands will possibly cross the entire grain in which the crack tip exists. There may be similar bands formed in other grains further away from the crack tip (Figure 2). Under strain cycling the dislocations move all along these bands and there will be a tendency to equalize the strain amplitude in an individual structural region in the RPZ. Therefore one should consider the crack tip area to be composed of these regions (hence forth called microstructural deformation zones or MDZ). All the elements in each MDZ can be assumed to have the same amount of cyclic plastic deformation. This

is schematically shown in Figure 3. In this figure the average position of a linear crack tip with respect to the matrix is shown. The actual MDZ size varies from one point to another on the crack tip, and an average size ($\bar{\rho}'$) will be considered in order to estimate FCGR. $\bar{\rho}'$ for the n-th order MDZ's ($\bar{\rho}'_n$) depends upon the microstructure or the distribution of the major deformation barriers. The average size of all the first order MDZ's ($\bar{\rho}_1'$) will be the average distance between the crack tip and the nearest barriers. When grain boundaries are the major barrier $\bar{\rho}_1'$ is equal to half of the grain size. For a material with large precipitates $\bar{\rho}_1'$ will be equal to half of their mean free path.

In order to estimate the strain amplitude for the elements in an MDZ ($\Delta\varepsilon_{pn}$) the following assumptions are made.

i) The crack blunts to a radius of r_o given by

$$r_o = \text{Crack-tip opening displacement} \div 2 = \frac{\Delta K^2}{\pi\sigma_y' 2}$$

where σ_y' is the cyclic yield strength ($\sim k'(0.004)^{n'}/2$), and the average n-th order zone begin at $x = r_{n-1}$ and ends at $x = r_n = r_o + \sum_{i=1}^{n} \bar{\rho}'_n$.

ii) The strain amplitude in a zone is equal to the average of the strain amplitude calculated for the zone from equation (6).

iii) The cross sectional area of the zone which is to be used for averaging will be bound by lines with equations $y = \pm Qx^q$ (see Figure 3). Since the shape of RPZ may be approximated to an ellipse, q can be taken to be equal to ½.

Then

$$\Delta\varepsilon_{pn} = \int_{x=r_{n-1}}^{r_n} x^{\frac{1}{2}} \cdot \Delta\bar{\varepsilon}_p \cdot dx \Big/ \int_{x=r_{n-1}}^{r_n} x^{\frac{1}{2}}\, dx \qquad (7)$$

Assuming ΔK to be constant, the total amount of strain cycling for an element before the crack tip arrives will be equal to the summation of the strain cycling of all the elements in the RPZ at one cycle. Therefore, for fracture the summation of the fraction of life per cycle for all of these elements should be unity. This fraction of fatigue life for an element in the n-th order MDZ will be given by the Coffin-Manson relation as:

$$\frac{1}{N_f} = 2\left(\frac{\Delta\varepsilon_{pn}}{2\varepsilon_f'}\right)^{-\frac{1}{c}}$$

where N_f is the number of cycles to failure for a specimen with a constant strain amplitude of $\Delta\varepsilon_{pn}$

Summing up all $\frac{1}{N_f}$ values for all the elements from 1st order MDZ to the end of the RPZ,

$$1 = \sum_{n=1}^{\infty} \frac{\bar{\rho}_n'}{da/dn} \cdot 2\left(\frac{\Delta\varepsilon_{pn}}{2\varepsilon_f'}\right)^{-\frac{1}{c}} \qquad (8)$$

or

$$\frac{da}{dn} = 2 \sum_{n=1}^{\infty} \bar{\rho}_n' \left(\frac{\Delta\varepsilon_{pn}}{2\varepsilon_f'}\right)^{-\frac{1}{c}}$$

where $\Delta\varepsilon_{pn}$ is given by equations (6) and (7).

Since the RPZ is finite, the contribution of higher order MDZ's will be negligible in most cases and equation (8) can be numerically solved.

The Threshold Phenomenon: At low ΔK the cyclic plastic deformation may be considered to be contained in the first order MDZ's. There exists a threshold for the plastic strain range ($\Delta\varepsilon_{p_{th}}$) below which deformation may be completely reversable and fatigue damage is not accumulated[21], and when ΔK is reduced some of the first order MDZ's will have $\Delta\varepsilon_{p1}$ (as calculated by equation 7) which will be smaller than $\Delta\varepsilon_{p_{th}}$. The crack tip will have to drag along these MDZ's and an accelerated reduction of CGR will be observed (Point B of Figure 1). When ΔK is further reduced (Point A of Figure 1), the majority of the first MDZ's will be deformed by cyclic strain smaller than $\Delta\varepsilon_{p_{th}}$ and the crack will not measurably grow. This will possibly be the case when the 1st order MDZ's with the size of average grain diameter have $\Delta\varepsilon_{p1} = \Delta\varepsilon_{p_{th}}$, and ΔK_{th} will be given by the relation:

$$\Delta\varepsilon_{p_{th}} = \int_{x=r_o}^{r_o+D} \Delta\bar{\varepsilon}_p \, x^{\frac{1}{2}} \, dx \Big/ \int_{x=r_o}^{r_o+D} x^{\frac{1}{2}} \, dx \qquad (9)$$

where $x = \dfrac{\Delta K_{th}^2}{(1+n')\pi E k'} \cdot \dfrac{1}{(\Delta\bar{\varepsilon}_p)^{n'+1} + \frac{k'}{E}(\Delta\bar{\varepsilon}_p)^{2n'}}$

and D = average grain diameter or particle spacing.

One may readily deduce from equation (9) that the threshold increases with increasing cyclic strength and increasing grain size.

Limitations of the Model: The major source of error for the calculations presented in this work is possibly in calculation of strain amplitudes for an MDZ (equation 7). Even if the consideration of an average size for each order MDZ is assumed to hold good, the calculation of $\Delta\varepsilon_{pn}$ by averaging the strain

amplitude obtained from equation (6) over one such average MDZ may not be appropriate. It is only a first approximation at best. (The reverse plastic zone size obtained by Rice's equation is found to be much smaller than actual measured zone sizes[22,23] indicating that his analysis may not hold good for the FCG experiments.) A more rigorous derivation of $\Delta\varepsilon_{pn}$ may be necessary.

The cyclic life-strain response (CLSR) and the cyclic stress-strain response (CSSR) of a material as obtained from a Low Cycle Fatigue (LCF) test may not be duplicated in the cyclic plastic zone of a FCP Test. Specifically, there is usually a break in both the $\Delta\varepsilon_p$ vs. N_f and $\Delta\sigma$ vs. $\Delta\varepsilon_p$ curves due to strain localization at low strain amplitudes of the LCF test.[24-27] However, it is the author's belief that if one plots the actual local response and not an overall response in the case of macroscopic strain localization, a more or less uniform CLSR and CSSR will be obtained for all $\Delta\varepsilon_p$ ranges if the mechanism involved is considered to be constant. Therefore to transfer LCF type data to FCP test predictions one should use data from the high strain amplitude range extrapolated to all ranges.

The predicted FCGR is for local crack growth behavior whereas the experimental data is usually for overall growth. In an FCP experiment the FCGR is measured along the overall crack growth direction whereas locally, the crack may or may not grow in the same direction. For a tortuous crack path the actual growth rate may be a factor of two or more higher than the measured overall growth. Therefore, it may be expected that for some cases the calculated growth rate may overestimate the measured growth value by this magnitude. If the crack is tortuous and one uses the standard equation for a straight crack normal to the stress axis, another apparent overestimation of FCGR by equation (8) will occur. Environmental factors have not been considered.

When considering the size of MDZ one has to consider the distribution of effective barriers. This may change from low ΔK level to high ΔK level. For single crystals and large grained materials the first MDZ size should be considered to be the plastic zone size.

CALCULATIONS AND DISCUSSION

The Effects of Various Parameters: Figure 4 shows the effect of various CSSR and CLSR parameters on FCGR. In each diagram only one variable is changed (at increments of 50%). Even though it is unlikely that only one parameter may be varied in an actual experiment, this figure allows one to observe the effect of considerable changes in a particular parameter. It is interesting to note that c has a larger effect than ε_f', and σ_y' has a larger effect than either n' or E. Figure 5a shows the effect of changing c and ε_f' in such a way that material 1 has the highest cyclic life at low $\Delta\varepsilon_p$ and material 3 has the highest cyclic life at high $\Delta\varepsilon_p$. It is found that the FCGR is lowest for material 1 at low ΔK, and for material 3 at high ΔK. Figure 5b shows the effect of changing σ_y' and n' in a similar fashion; however, the effect of this change on FCGR seems negligible for any ΔK range.

Figure 6 shows the effect of the changes in microstructure. For the model presented here the microstructural parameter, ρ' has a strong effect provided the other parameters do not change (Figure 6a). For most materials both σ_y' and ε_f' (and possibly n' and c) will change with ρ'. If σ_y' increases with decreasing ρ' the predicted curves may appear as shown in Figure 6b. If ε_f' increases with decreasing ρ' the changes will be given by Figure 6c. Figure 6b and 6c show that the microstructure may not have a significant effect on overall FCGR. Figure 6d shows that if both σ_y' and ε_f' are assumed to improve by reducing ρ', the effect of changing ρ' may be completely offset by the change of

σ_y' and ε_f'. Therefore, it is clear from Figure 6 that changes in ρ' may create confusing effects on FCGR if its effect on cyclic response parameters is ignored.

Since it is not possible to change any one parameter without some changes in at least another parameter, and since none of these parameters are negligible, this model shows that all of them must be considered for observing changes in FCGR. Furthermore there may be a dynamic interaction between crack growth, stress intensity-factor range, frequency of loading, microstructure, materials cyclic response and environment; and various factors must be isolated to make any conclusions about FCP behavior.

Comparison with Experimental FCGR data: Figure 7a shows a comparison between the experimentally measured FCGR for a Ti-24% V as quenched alloy[28] and that calculated from equation (8) using low cycle fatigue parameters[24]. The calculated curve is well within the normal experimental scatterband. The same alloy was also heat treated to change the microstructure by precipitating α particles in the β matrix. In this case also the calculated curve very accurately predicts the FCGR[28]. The calculated FCGR for AISI 304 stainless steel and Ti-6-4 using the LCF data of smith et al.[29] fall within the scatterband of the experimentally measured rate obtained by Shahinian et al.[30] and Irving and Beevers[31] respectively.

SUMMARY

The fatigue crack growth (FCG) behavior of a material has been shown to be related to its cyclic stress strain response (CSSR) and cyclic life strain response (CLSR) and its microstructure. It has been proposed that the reverse plastic zone (RPZ) can be divided into small microstructural deformation zones (MDZ) within which the cyclic deformation may be considered uniform. A comparison

between experimental and calculated curves show excellent agreement. This is significant when one considers that the model predicts the fatigue crack growth behavior from the low cycle fatigue data and the microstructure of the material without using any adjustable parameters.

ACKNOWLEDGEMENTS

The author wishes to acknowledge Dr. E. A. Starke, Jr. for his contributions in all phases of the development of this paper. Mr. E. J. Coyne, Jr. and Dr. S. Spooner helped in computer programming. This research was supported by the Office of Naval Research (U.S.A.) under Contract N00014-75-C-0349, Dr. Bruce A. McDonald Contract Monitor. The United States Government is authorized to reproduce and distribute reprints for Government purposes notwithstanding any copyright notation herein.

REFERENCES

1. P. C. Paris, M. P. Gomez and W. E. Anderson, "The Trend in Engineering," University of Washington 13, 9 (1961).

2. P. C. Paris and F. Erdogan, "Transactions of the ASME, Journal of Basic Engineering 85, 528 (1963).

3. S. R. Swanson, F. Cicci and W. Hoppe, Fatigue Crack Propagation, ASTM STP No. 415, 312 (1967).

4. D. P. Wilhelm, Fatigue Crack Propagation, ASTM STP No. 415, 363 (1967).

5. J. Schijve, Fatigue Crack Propagation, ASTM STP No. 415, 415 (1967).

6. L. P. Pook, A Stress Analysis and Growth of Cracks, ASTM STP No. 513, 106 (1971).

7. J. Weertman, Int. J. Fract. 9, 125 (1973).

8. T. Mura and C. T. Lin, Int. J. Fract. 20, 284 (1974).

9. J. R. Rice, Fatigue Crack Propagation, ASTM STP No. 415, 247 (1967).

10. G. P. Cherepanov and H. Halmanov, Eng. Fract. Mech. 4, 219 (1972).

11. *P. E. Irving and L. N. McCartney*, Metal Sciences 11, 351 (1977).

12. S. Majumdar and J. Morrow: University of Illinois, T&A.M. Report No. 364 (1973).

13. H. W. Liu and N. Iino, Proc. 2nd Int. Conf. on Fract., Chapman and Hall, p 812 (1969).

14. F. A. McClintock, ASTM STP No. 415 (1967). Discussion to article by C. Laird, p. 170.

15. R. W. Larder, Phil. Mag. 17, 71 (1968).

16. H. W. Lin, Trans, ASME 85, 116 (1963).

17. N. E. Frost and J. R. Dixon, Int. J. Fract. 3, 301 (1967).

18. M. A. Miner, J. Appl. Mech. 12A, 159 (1945).

19. L. F. Coffin, Jr., Trans. ASME 76, 931 (1954).

20. S. S. Manion and H. M. Hirschberg, "Fatigue-An Interdisciplinary Approach," ed. by J. J. Burke, N. L. Reed, and V. Weiss, Syracuse University Press, p. 133 (1964)

21. P. Lukas and T. Polak, "Work Hardening in Tension and Fatigue," ed. A Thompson, Mech. Met. Committee of TMS-AIME p. 177 (1975).

22. Y. Izumi, Ph.D. Thesis, Northwestern University, June 1978.

23. S. Ikeda, Y. Izumi and M. E. Fine, Eng. Fract. Mech. 9, 123 (1977).

24. S. B. Chakrabortty, T. K. Mukhopadhyay, and E. A. Starke, Jr., Acta Met. (in press).

25. T. H. Sanders, Jr. and E. A. Starke, Jr., Met. Trans. A 7A, 1407 (1976).

26. R. E. Sanders, Jr. and E. A. Starke, Jr., Mat. Sci. Engng. 28, 53 (1977).

27. A. Saxena and S. D. Antalovitch, Met. Trans. A. 6A, 1809 (1975).

28. S. B. Chakrabortty and E. A. Starke, Jr., to be published.

29. R. W. Smith, M. H. Hirschberg, and S. S. Manson, NASA TN D-1574 (1963).

30. P. Shahinian, H. E. Watson and H. H. Smith, J. of Materials 1, 527 (1972).

31. P. E. Irving and C. J. Beevers, Met. Trans. 5, 391 (1974).

LIST OF FIGURES

Figure 6. The Calculated Fatigue Crack Propagation Rate Versus Stress Intensity Factor Range Curves Showing the Effect of Changing ρ'.

(a) Without corresponding changes in any other parameter. $c = -0.66$, $\varepsilon_f' = 1$, $\sigma_y' = 620$ MPa, $n' = 0.12$, $E = 211$ GPa, and $\rho' = 2$ μm (curve 1); 10 μm (curve 2); 50 μm (curve 3); 0.5 μm (curve 4).

(b) σ_y' changes with ρ' with the relation: $\sigma_y' = (350 + 0.86/\sqrt{\rho'})$ MPa. $c' = -0.66$, $\varepsilon_f' = 1.0$, $n' = 0.12$, $E = 211$ GPa and $\rho' = 2$ μm (curve 1); 10 μm (curve 2); 50 μm (curve 3); 0.5 μm (curve 4).

(c) ε_f' changes with ρ' by a relation: $\varepsilon_f' = 0.2 + 2.5 \times 10^{-3}/\sqrt{\rho'}$. $c = -0.66$, $\sigma_y' = 620$ MPa, $n' = 0.12$, $E = 211$ GPa and $\rho' = 2$ μm (curve 1); 10 μm (curve 2); 50 μm (curve 3); 0.5 μm (curve 4).

(d) Both ε_f' and σ_y' changes with ρ' by the relations: $\varepsilon_f' = 0.2 + 2.5 \times 10^{-3}/\sqrt{\rho'}$, and $\sigma_y' = (350 + 0.86/\sqrt{\rho'})$ MPa. $c = -0.66$, $n' = 0.12$, $E = 211$ GPa and $\rho' = 2$ μm (curve 1); 10 μm (curve 2); 50 μm (curve 3); 0.5 μm (curve 4).

Figure 7. Calculated and Experimental Fatigue Crack Growth Rate Versus Stress Intensity Factor Range Curves.

(a) For a Ti-24V solutionized and quenched alloy[24,28], $c = -0.8$, $\varepsilon_f' = 0.65$, $\sigma_y' = 860$ MPa, $n' = 0.06$, $E = 110$ GPa, $\rho' = 32$ μm. The calculated FCGR is shown by solid lines. Experimental data[28] is given by crosses.

(b) For a cold worked 304 stainless steel.[29,30] $c = -0.7$, $\varepsilon_f' = 1$, $\sigma_y' = 760$ MPa, $n' = 0.14$, $\rho' = 35$ μm, $E = 211$ GPa. The calculated FCGR is shown by solid line and the best fit experimental curve[30] is shown by dotted line.

(c) For a Ti-6Al-4V alloy in martensitic condition[29,31]. $c = -0.7$, $\varepsilon_f' = 1$, $\sigma_y' = 880$ MPa, $n' = 0.086$, $\rho = 2.5$ μm, $E = 120$ GPa. The calculated FCGR is given by solid lines. The best fit experimental curve[31] is shown by dotted line.

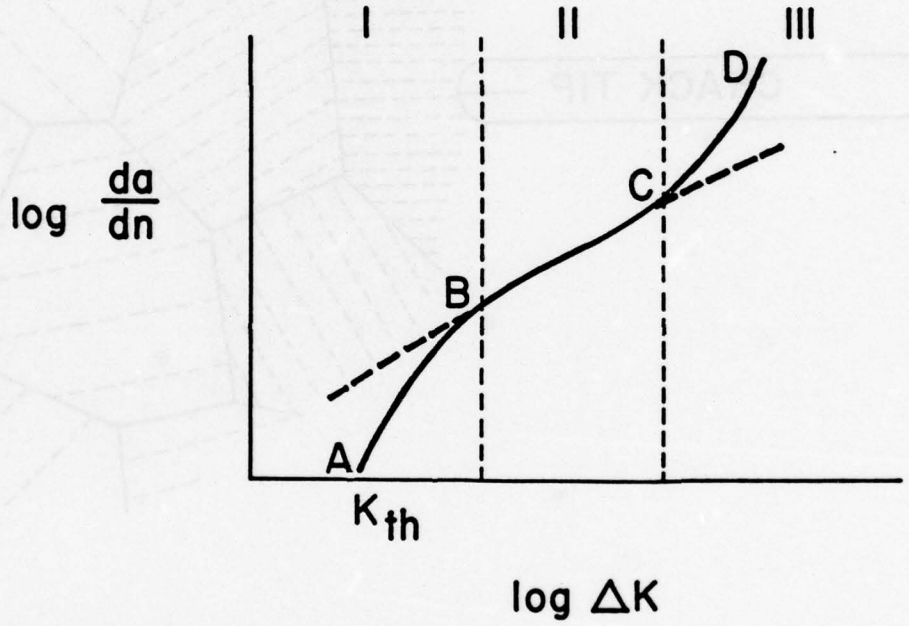

Figure 1. Schematic Representation of A Typical Crack Growth Rate Versus Stress Intensity Range Curve.

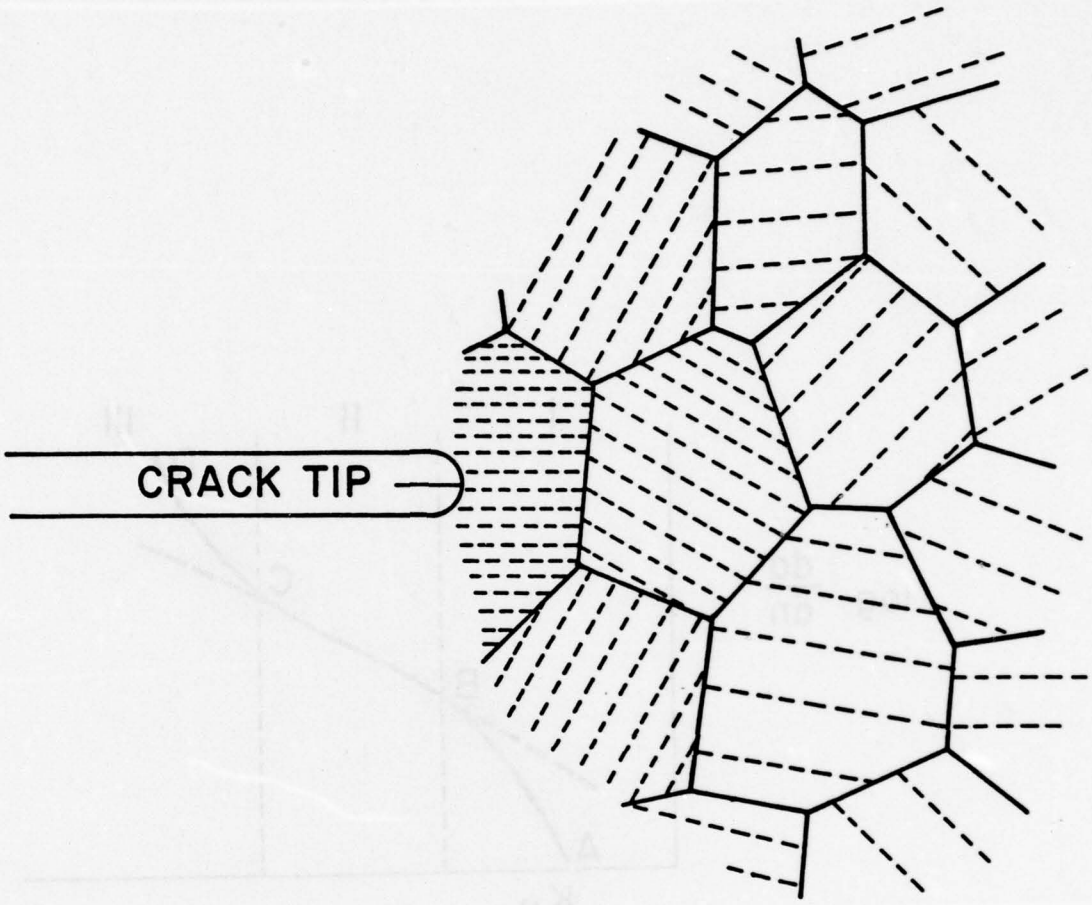

Figure 2. A Schematic Representation of the Structure of Fatigue Crack-Tip Area. The Extent of Cyclic Deformation is Represented by the Density of Dotted Lines.

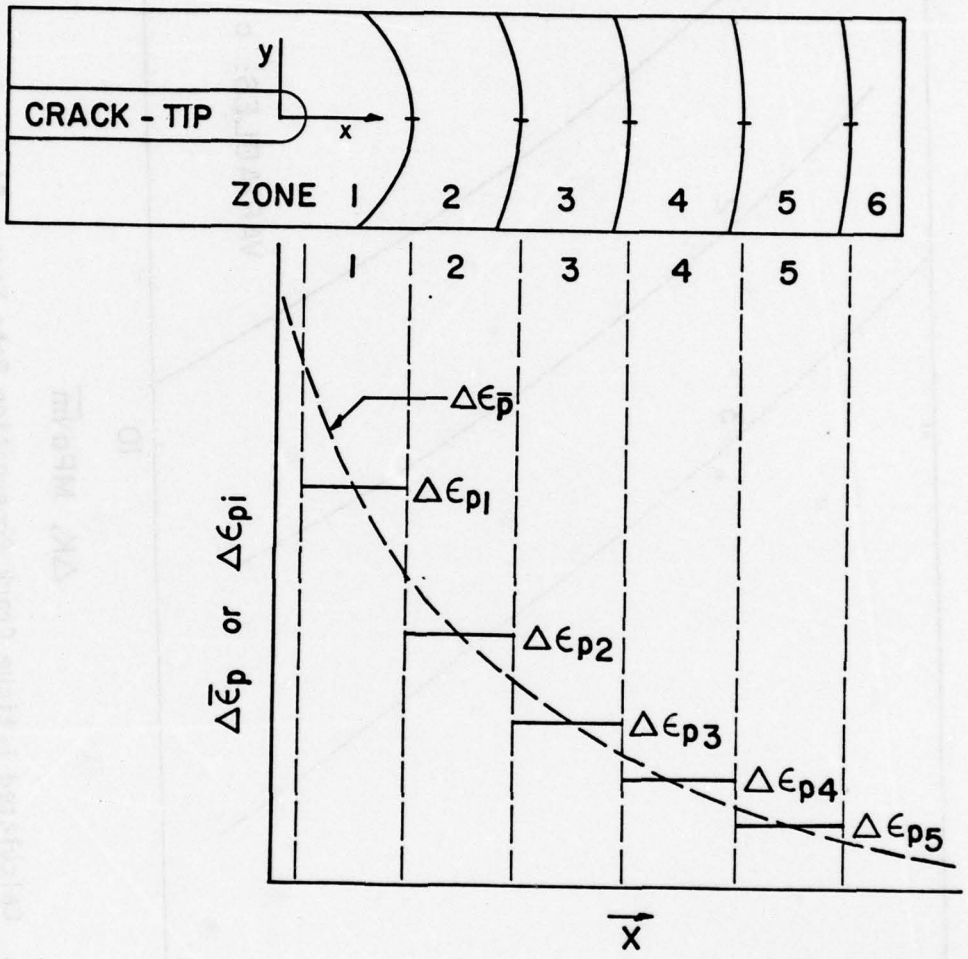

Figure 3. Schematic Representation of Average Microstructural Deformation Zones and Their Plastic Strain Amplitudes ($\Delta\epsilon_{pn}$, n=1,2,3...). The Estimated Plastic Strain Amplitude for a Continuum is Shown by the Dotted Line.

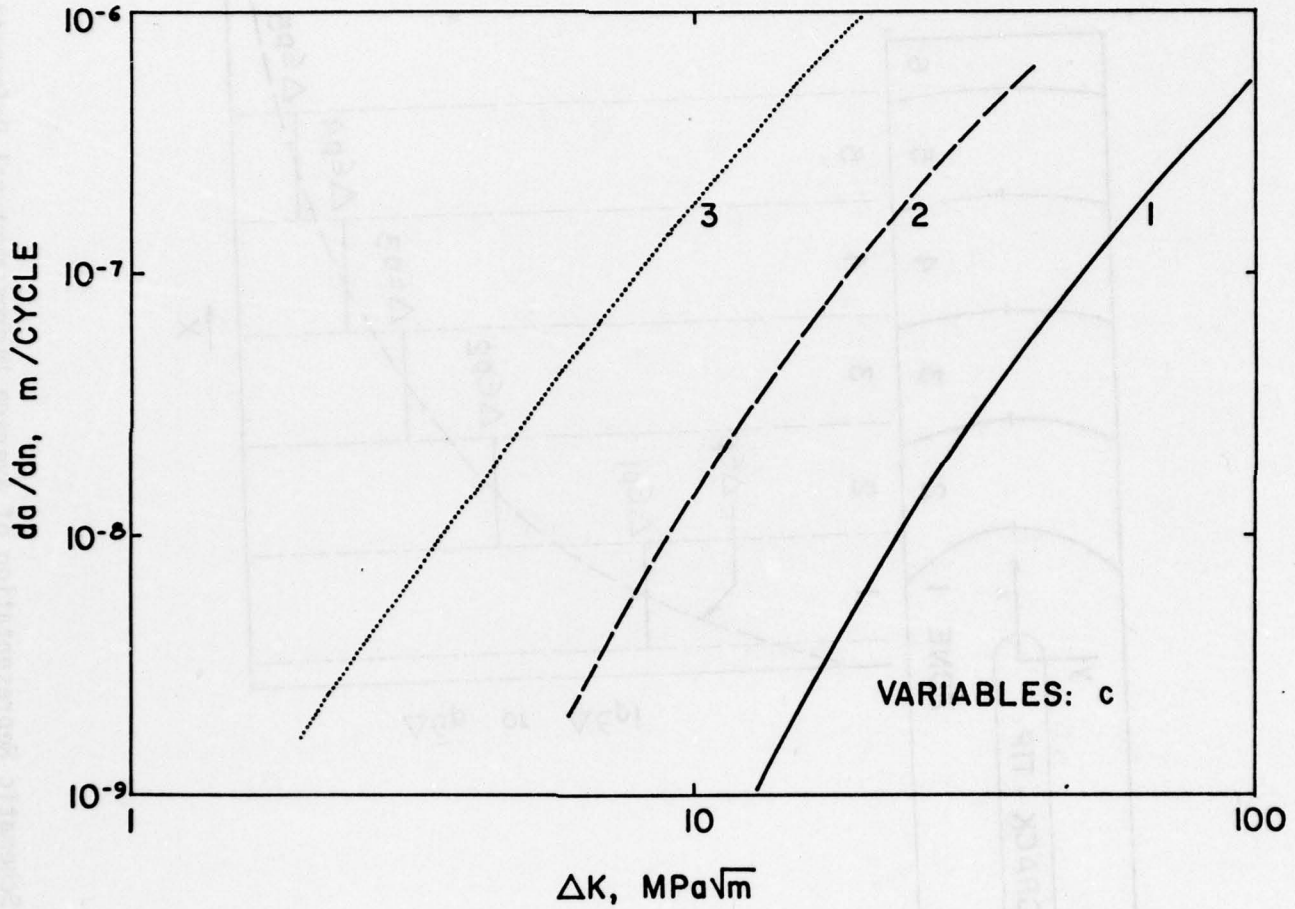

Figure 4. Calculated Fatigue Crack Propagation Rate Versus Stress Intensity Range Curves Showing the Effect of Changing Various Individual Cyclic Stress-Strain and Life-Strain Response Parameters.

(a) ε_f' = 1, σ_y' = 620 MPa, n' = 0.12, E = 211 GPa, ρ' = 10 μm and c = -0.44 (curve 1); -0.66 (curve 2); -0.99 (curve 3).

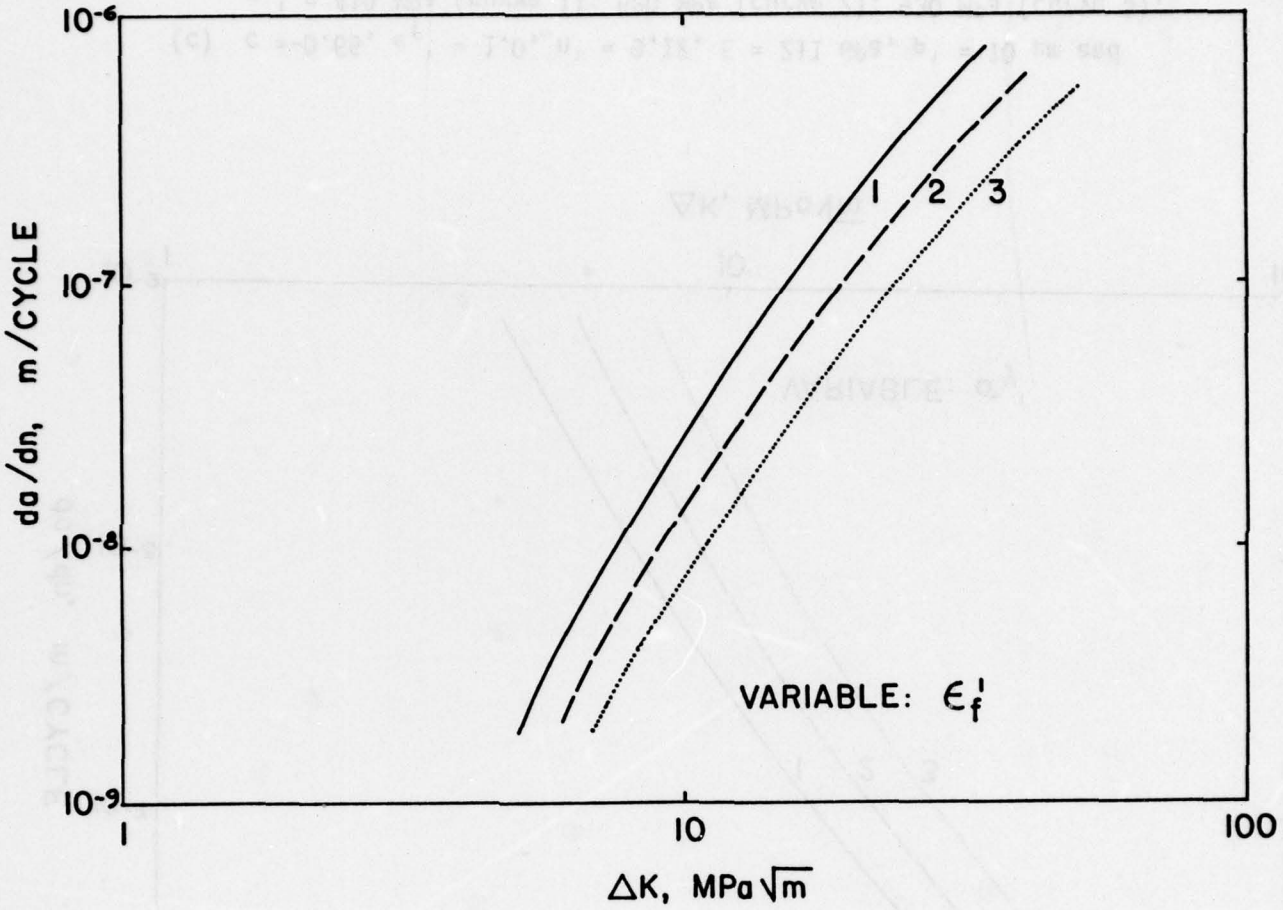

(b) c = -0.66, σ_y' = 620 MPa, n' = 0.12, E = 211 GPa, ρ' = 10 μm and ϵ_f' = 0.66 (curve 1); 1.0 (curve 2); 1.5 (curve 3).

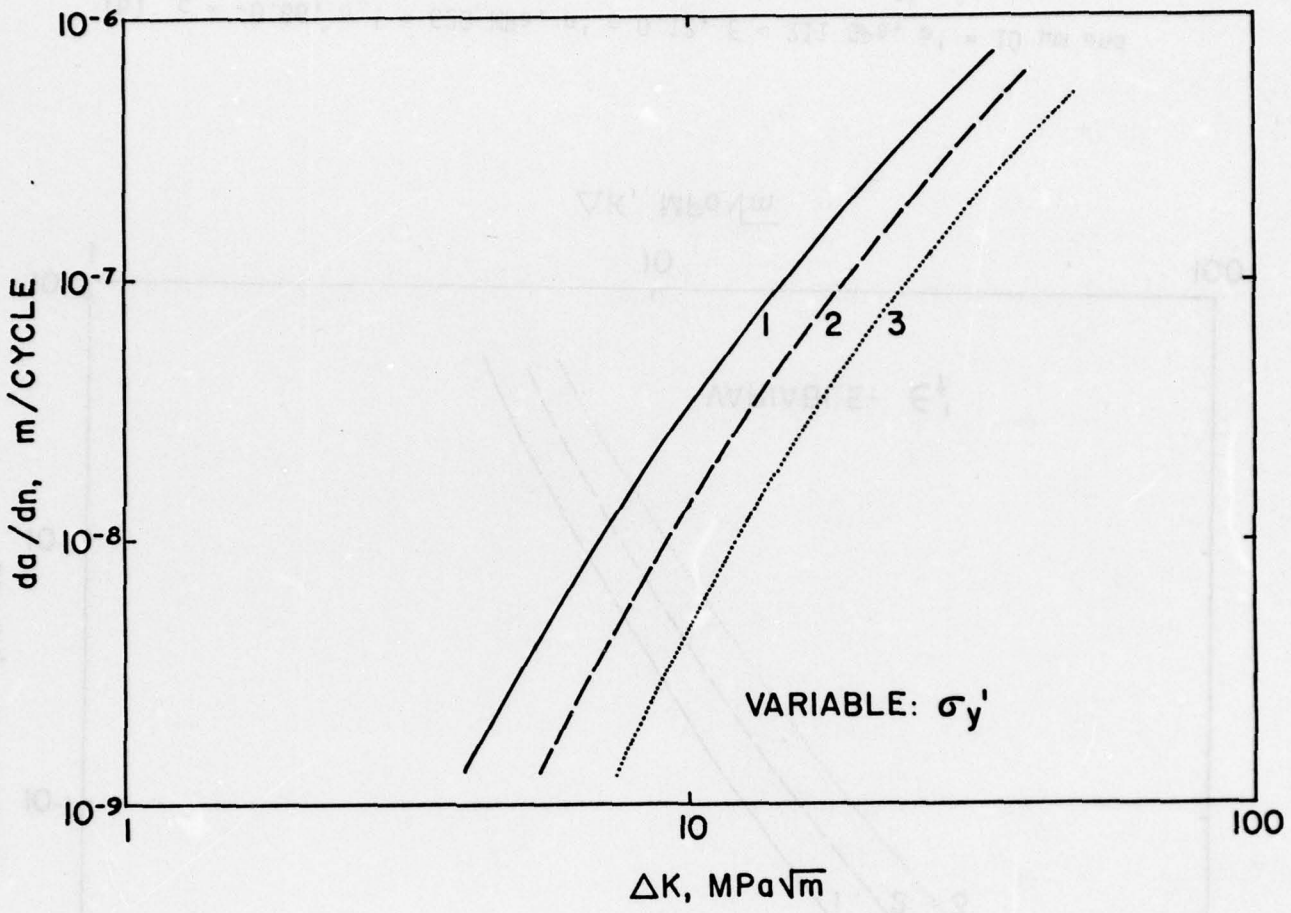

(c) c =-0.66, ε_f' = 1.0, n' = 0.12, E = 211 GPa, ρ' = 10 μm and σ_y' = 410 MPa (curve 1); 620 MPa (curve 2); 930 MPa (curve 3).

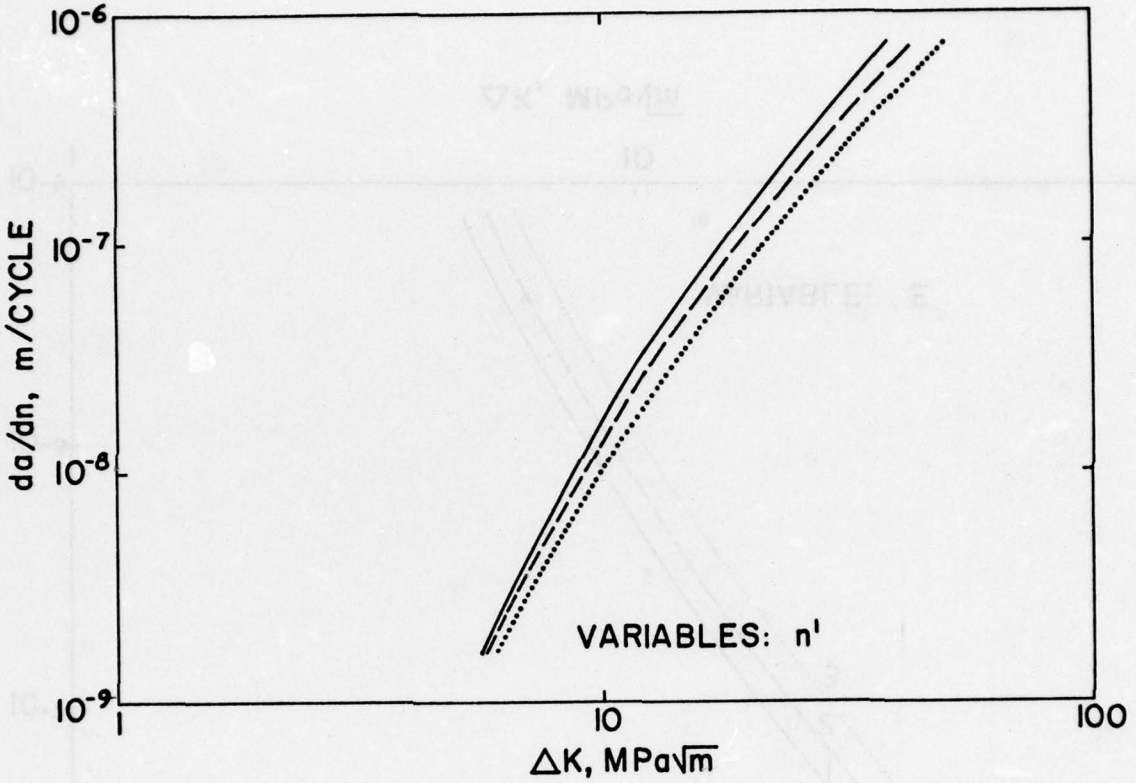

(d) c = -0.66, ε_f' = 1.0, σ_y' = 620 MPa, E = 211 GPa, ρ' = 10 μm and n' = 0.08 (curve 1); 0.12 (curve 2); 0.18 (curve 3).

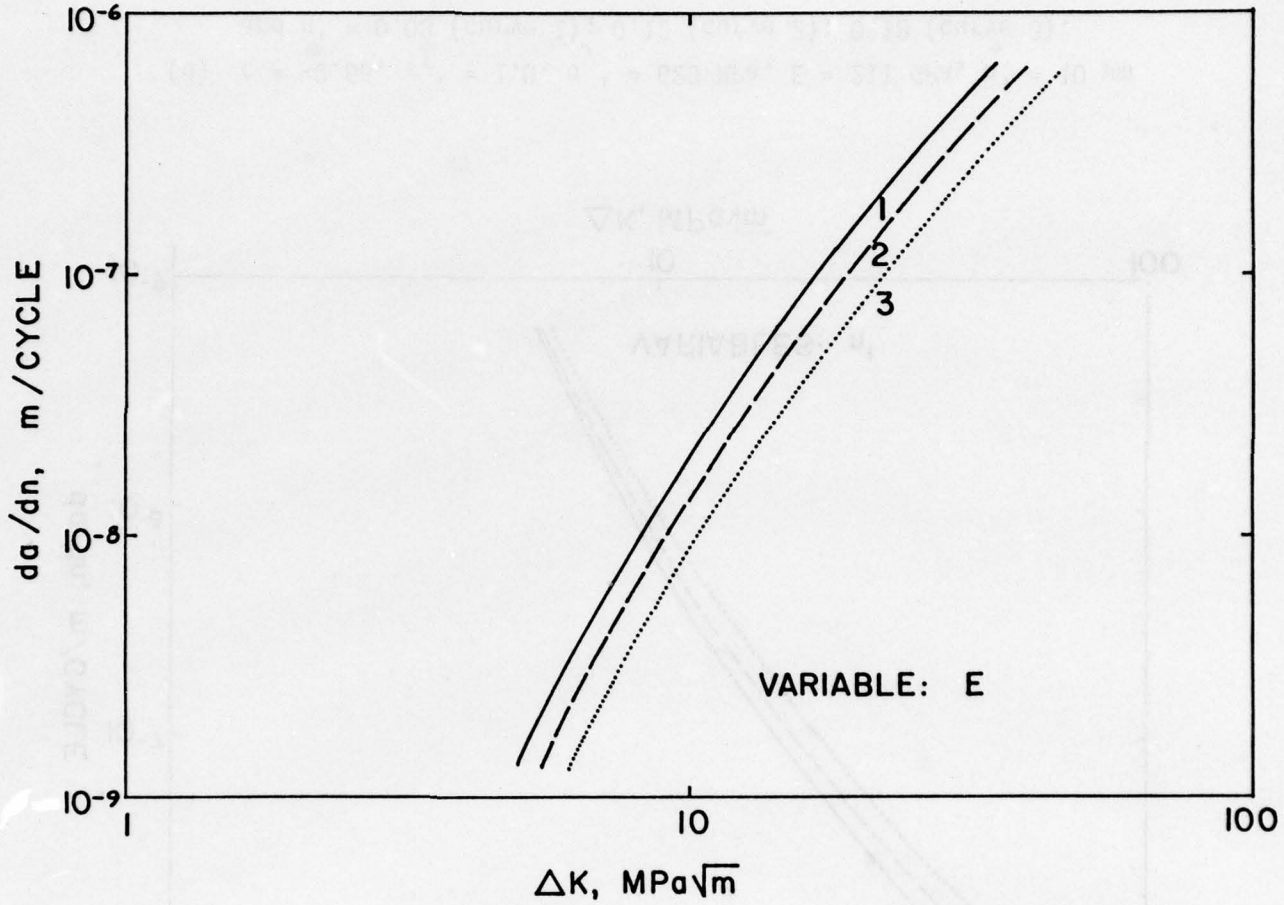

(e) $c = -0.66$, $\varepsilon_f' = 1.0$, $\sigma_y' = 620$ MPa, $n' = 0.12$, $\rho' = 10$ μm and $E = 141$ GPa (curve 1); 211 GPa (curve 2); 317 GPa (curve 3).

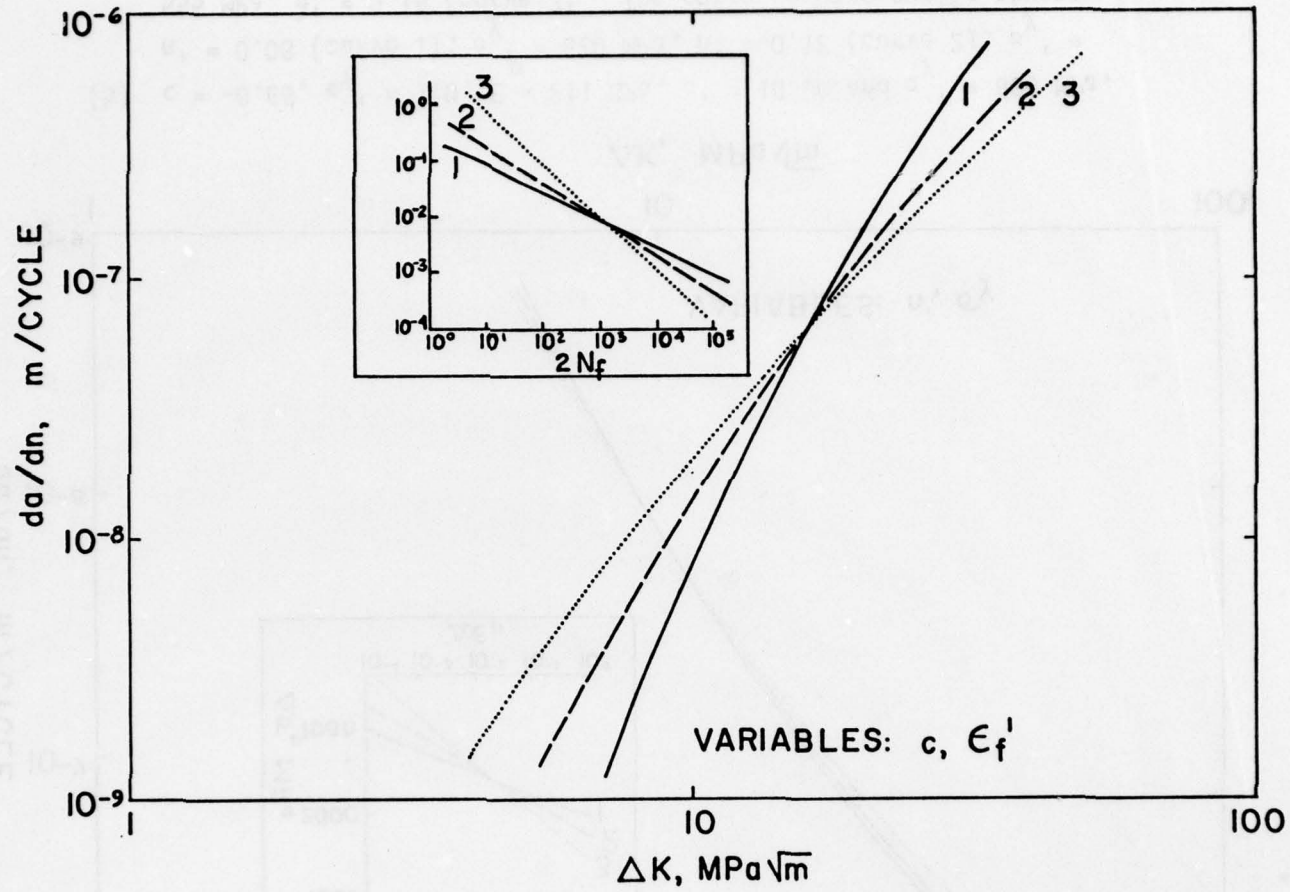

Figure 5. The Calculated Crack Propagation Rate Versus Stress Intensity Factor Range Curves Showing the Effects of Changing Two Cyclic Response Parameters Simultaneously:

(a) σ_y' = 620 MPa, n' = 0.12, E = 211 GPa, ρ' = 10 μm and c = -0.44, ε_f' = 0.25 (curve 1); c = -0.66, ε_f' = 1 (curve 2); c = -0.99, ε_f' = 9 (curve 3). The corresponding Coffin-Manson Plots are shown in the insert.

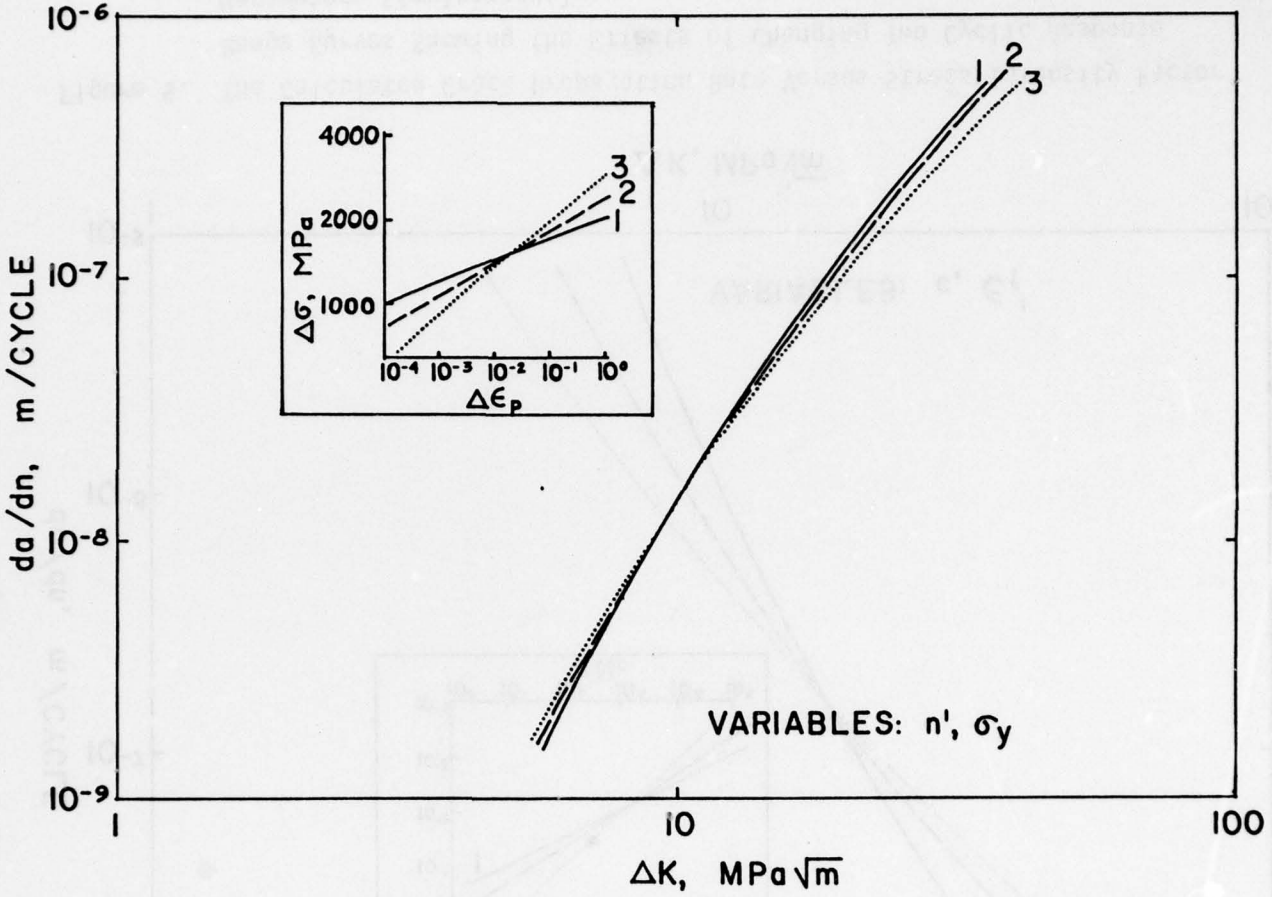

(b) c = -0.66, ε_f' = 1.0, E = 211 GPa, ρ' = 10 μm and σ_y' = 660 MPa, n' = 0.08 (curve 1); σ_y' = 620 MPa, n' = 0.12 (curve 2); σ_y' = 555 MPa, n' = 0.18 (curve 3). The corresponding cyclic stress strain curves are shown in the insert.

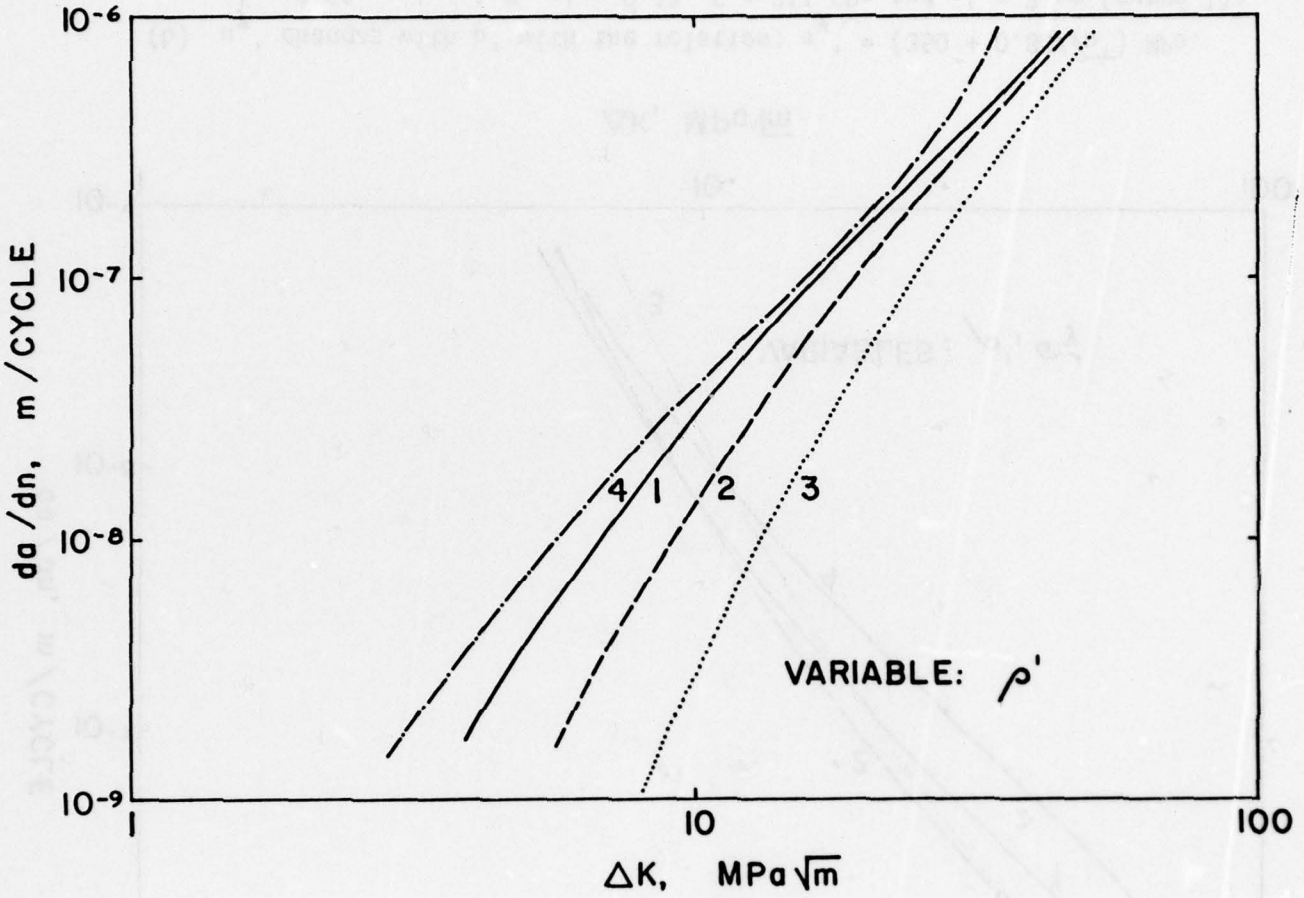

Figure 6. The Calculated Fatigue Crack Propagation Rate Versus Stress Intensity Factor Range Curves Showing the Effect of Changing ρ'.

(a) Without corresponding changes in any other parameter. $c = -0.66$, $\varepsilon_f' = 1$, $\sigma_y' = 620$ MPa, $n' = 0.12$, $E = 211$ GPa, and $\rho' = 2$ μm (curve 1); 10 μm (curve 2); 50 μm (curve 3); 0.5 μm (curve 4).

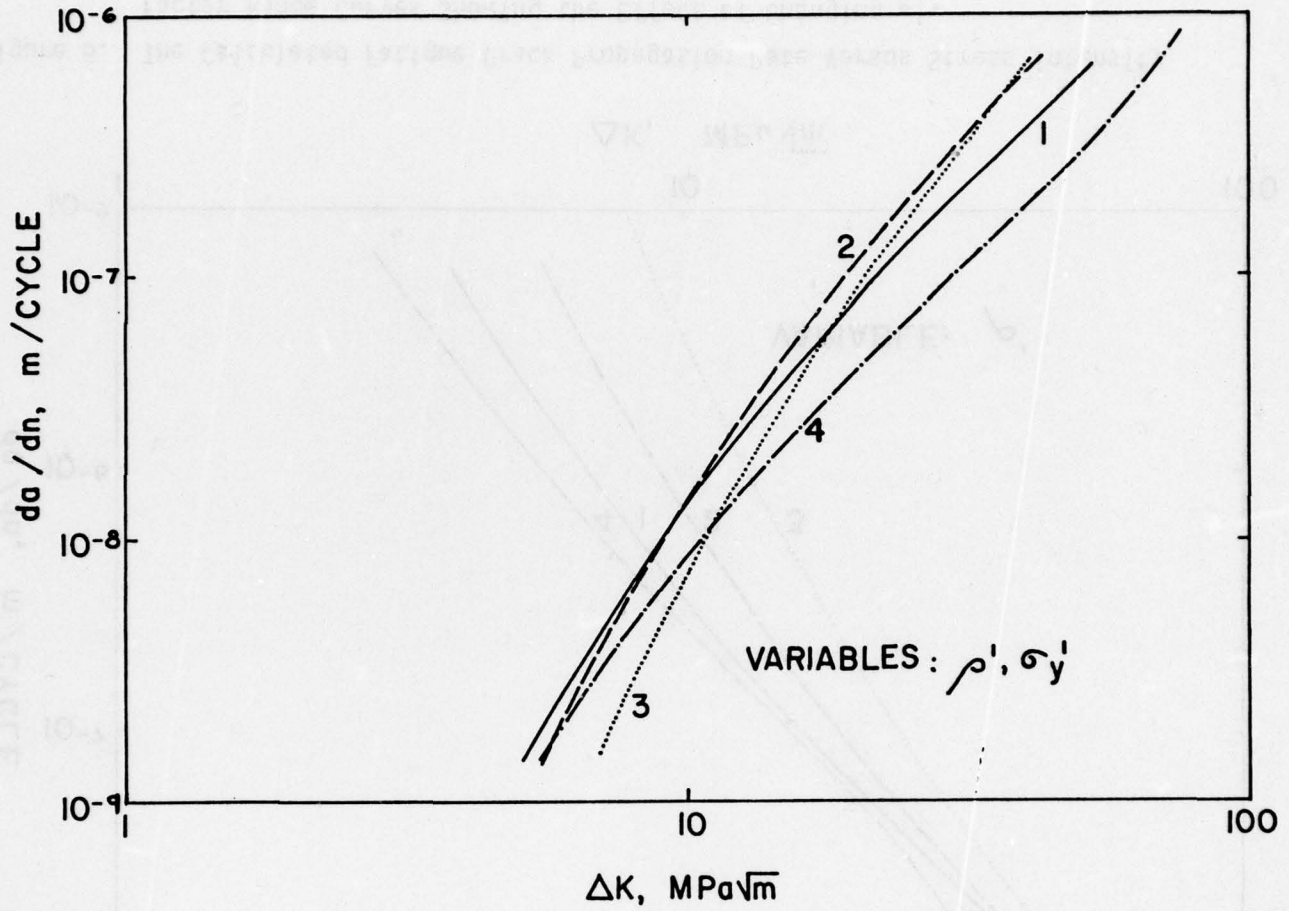

(b) σ_y' changes with ρ' with the relation: $\sigma_y' = (350 + 0.86/\sqrt{\rho'})$ MPa. $c' = -0.66$, $\varepsilon_f' = 1.0$, $n' = 0.12$, $E = 211$ GPa and $\rho' = 2$ μm (curve 1); 10 μm (curve 2); 50 μm (curve 3); 0.5 μm (curve 4).

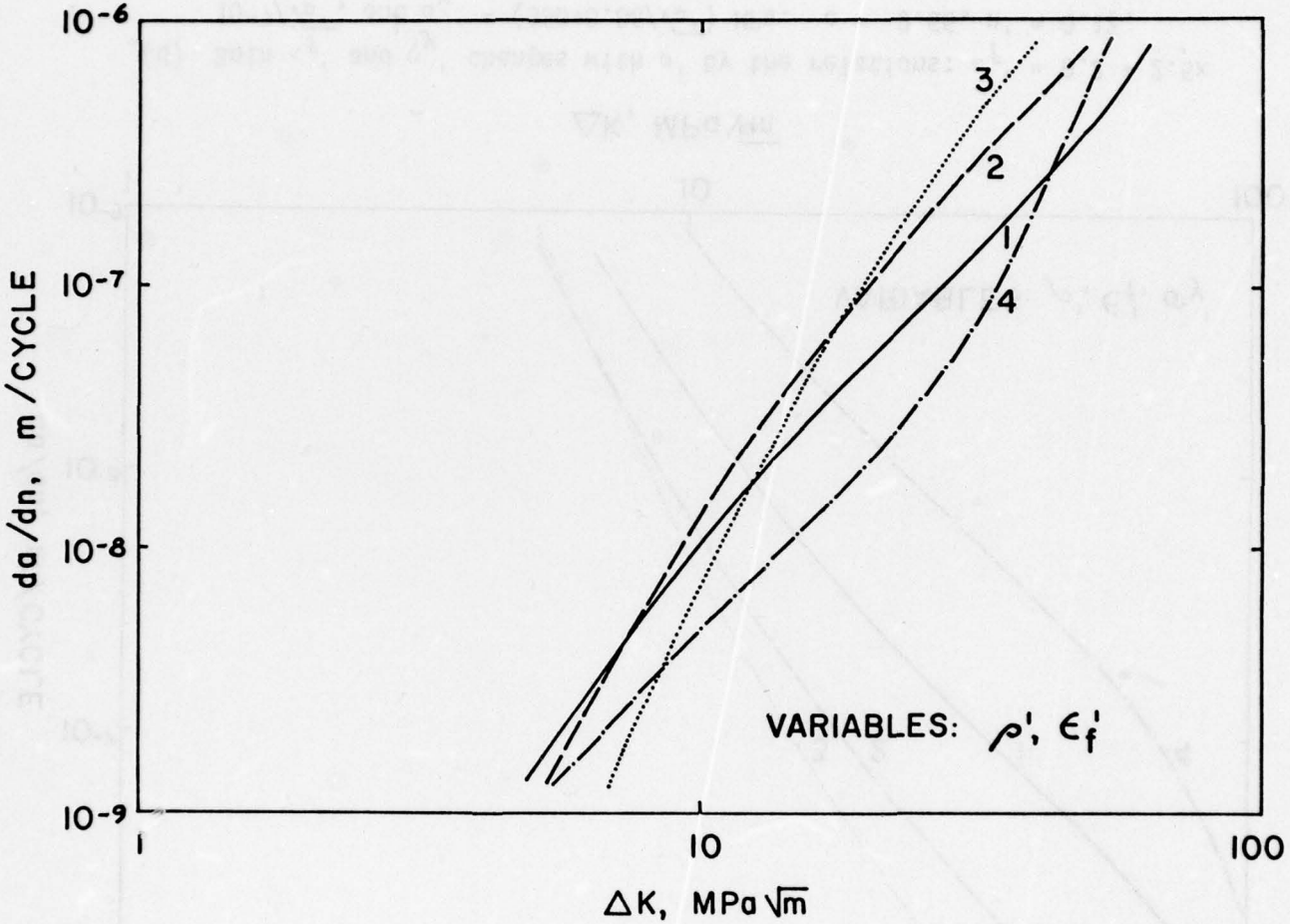

(c) ε_f' changes with ρ' by a relation: $\varepsilon_f' = 0.2 + 2.5\times10^{-3}/\sqrt{\rho'}$. $c = -0.66$, $\sigma_y' = 620$ MPa, $n' = 0.12$, $E = 211$ GPa and $\rho' = 2$ μm (curve 1); 10 μm (curve 2); 50 μm (curve 3); 0.5 μm (curve 4).

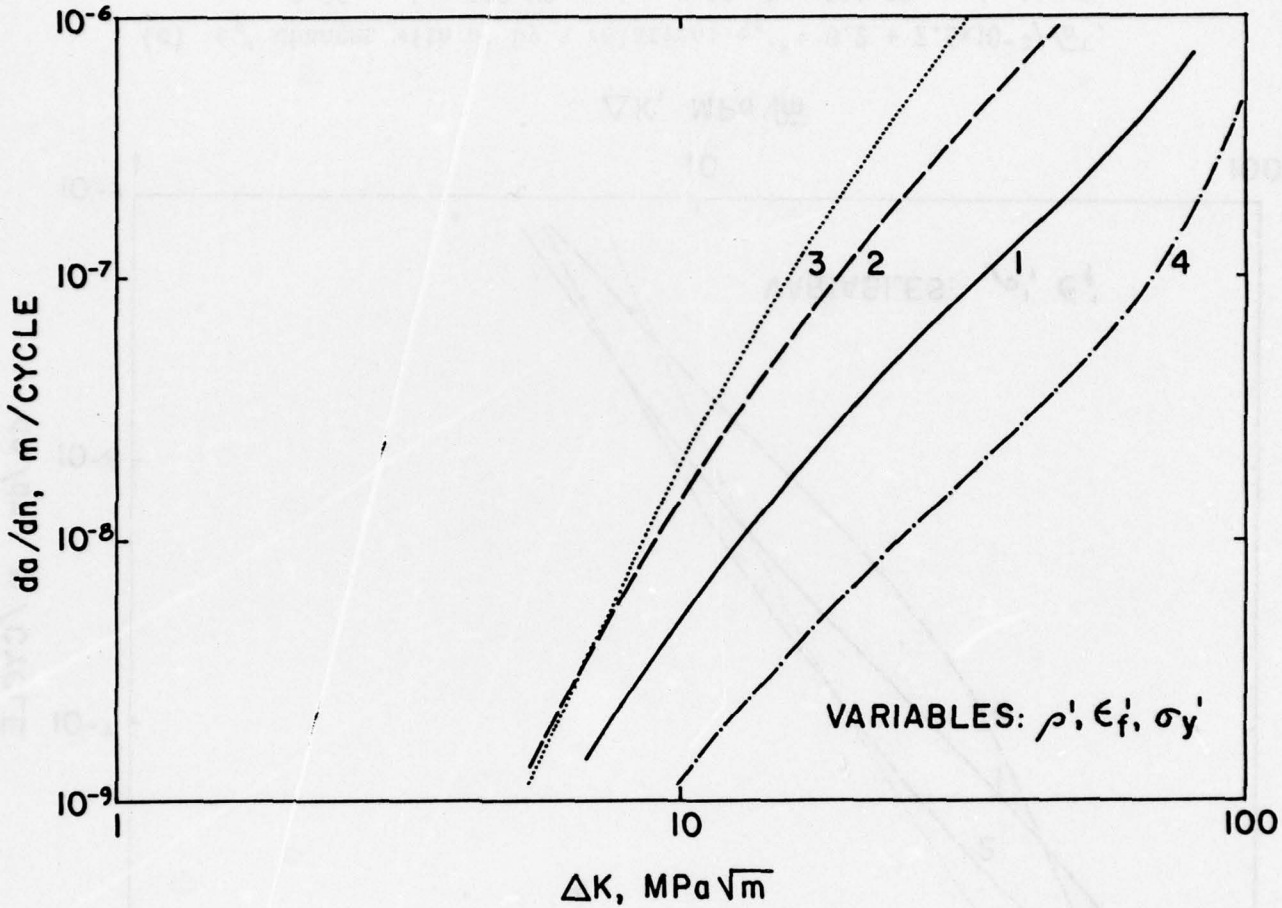

(d) Both ε_f' and σ_y' changes with ρ' by the relations: $\varepsilon_f' = 0.2 + 2.5 \times 10^{-3}/\sqrt{\rho'}$, and $\sigma_y' = (350+0.86/\sqrt{\rho'})$ MPa. c = -0.66, n' = 0.12, E = 211 GPa and ρ' = 2 μm (curve 1); 10 μm (curve 2); 50 μm (curve 3); 0.5 μm (curve 4).

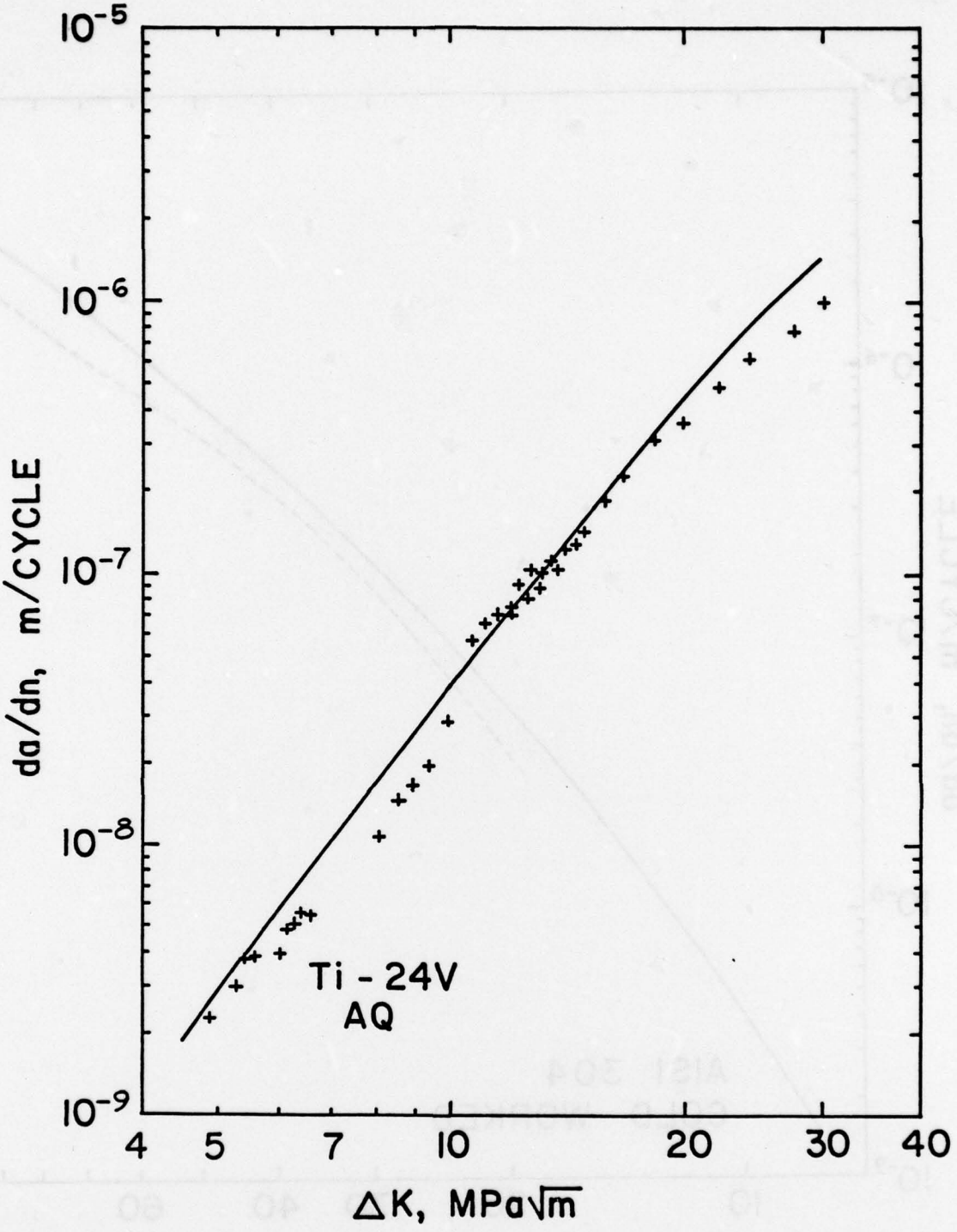

Figure 7. Calculated and Experimental Fatigue Crack Growth Rate Versus Stress Intensity Factor Range Curves.

(a) For a Ti-24V solutionized and quenched alloy[24,28], c = -0.8, ε_f' = 0.65, σ_y' = 860 MPa, n' = 0.06, E = 110 GPa, ρ' = 32 μm. The calculated FCGR is shown by solid lines. Experimental data[28] is given by crosses.

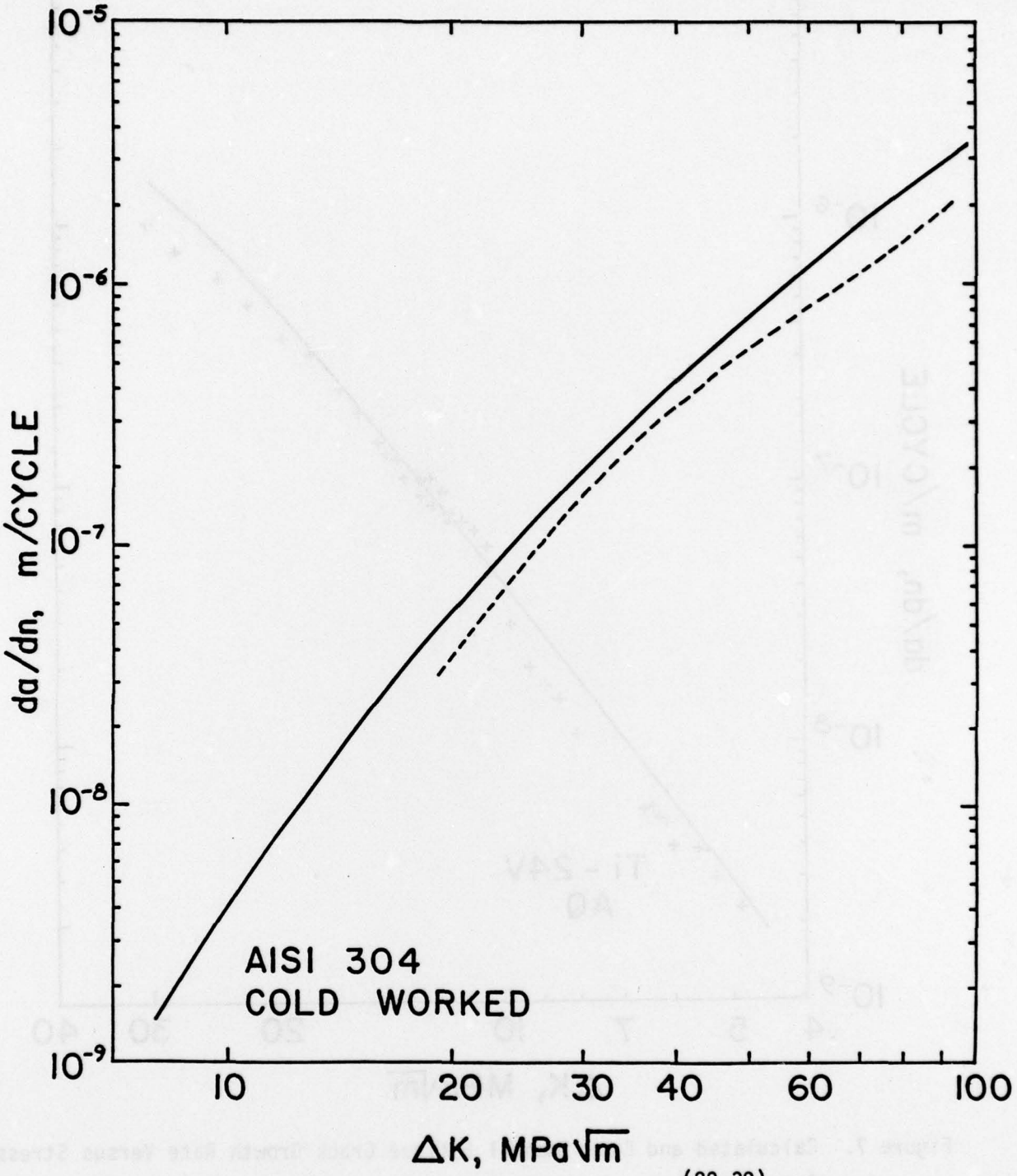

(b) For a cold worked 304 stainless steel.[29,30] $c = -0.7$, $\varepsilon_f' = 1$, $\sigma_y' = 760$ MPa, $n' = 0.14$, $\rho' = 35$ μm, $E = 211$ GPa. The calculated FCGR is shown by solid line and the best fit experimental curve[30] is shown by dotted line.

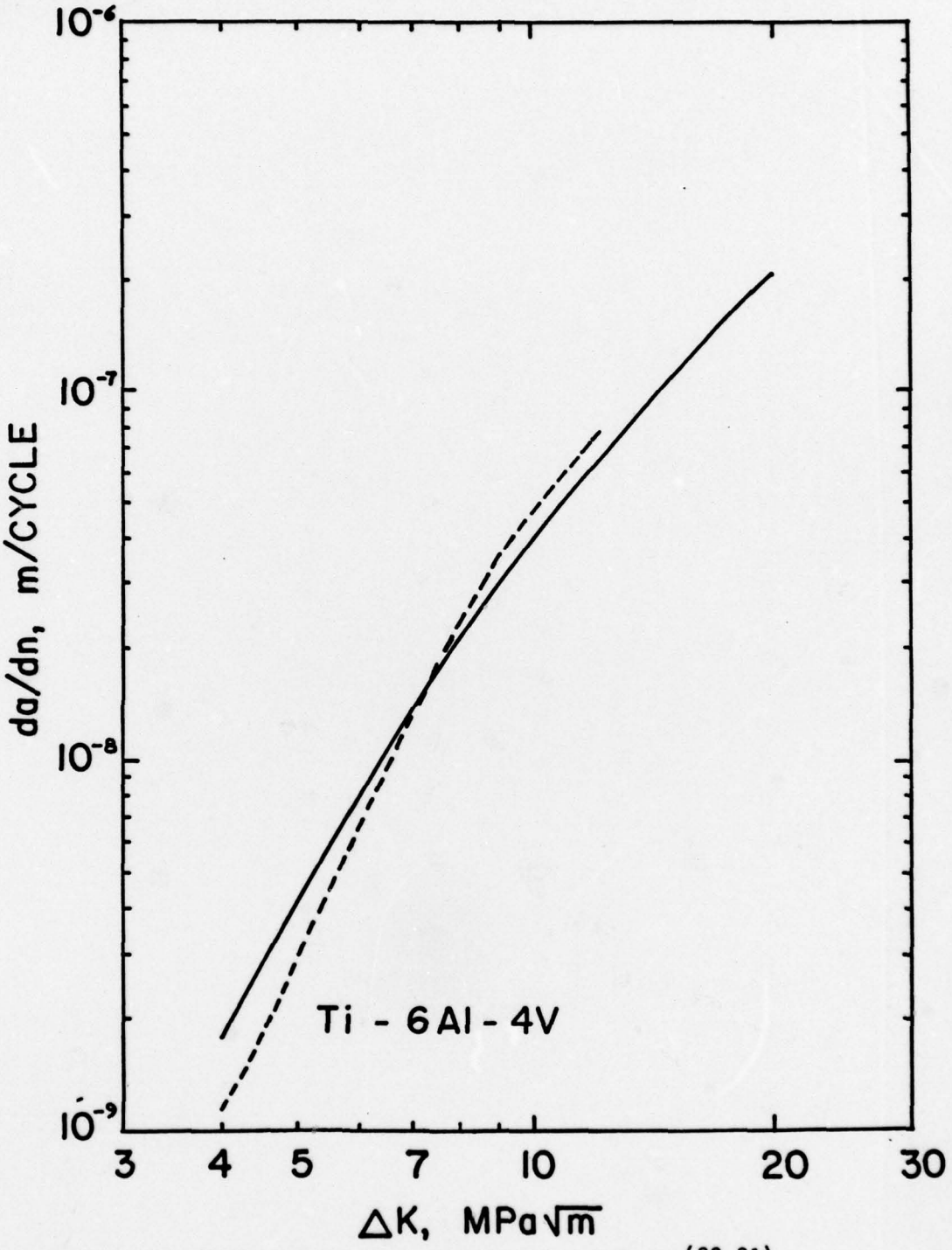

(c) For a Ti-6Al-4V alloy in martensitic condition[29,31]. c = -0.7, ε_f' = 1, σ_y' = 880 MPa, n' = 0.086, ρ = 2.5 μm, E = 120 GPa. The calculated FCGR is given by solid lines. The best fit experimental curve[31] is shown by dotted line.


ED
78